Rare Metal Materials and Engineering
Volume 54, Issue 9, September 2025
Available online at www.rmme.ac.cn

Science Press

Cite this article as: Guo Xuyan, Xiong Zhuangzhuang, Wang Guixiang, et al. Influence of Current Density and Copper Ion Concentration on Properties of Electrodeposited Cu-Ni Coatings[J]. Rare Metal Materials and Engineering, 2025, 54(09): 2231-2240. DOI: https://doi.org/10.12442/j.issn.1002-185X.20240460.

ARTICLE

Influence of Current Density and Copper Ion Concentration on Properties of Electrodeposited Cu-Ni Coatings

Guo Xuyan[1], Xiong Zhuangzhuang[1], Wang Guixiang[1,3], Zhou Qiang[1], Wu Yanxiong[1], Kong Delong[2], Ma Fuqiu[1], Wu Ruizhi[3]

[1] Yantai Research Institute, Harbin Engineering University, Yantai 264006, China; [2] Chemical Engineering and Materials Science, Zaozhuang University, Zaozhuang 277160, China; [3] Key Laboratory of Superlight Materials and Surface Technology, Harbin Engineering University, Harbin 150001, China

Abstract: A straightforward, highly effective, and environmentally friendly technique was investigated for protecting carbon steel surfaces from corrosion, i. e., depositing Cu-Ni alloy coatings on the workpiece's surface to impede corrosive medium. The effects of current density and copper ion concentration (Cu^{2+}) on the composition, morphology, and properties of the coating were analyzed using scanning electron microscope, X-ray energy dispersive spectrometer, Vickers hardness tester, friction and wear tester, and electrochemical testing. Results show that a cauliflower-like Ni-rich protrusion structure appears on the coating surface. The lower current density and Cu^{2+} concentration affect the Vickers hardness and wear resistance of the coating by altering the microstructure and Cu/Ni content, both leading to a decrease in hardness and wear resistance. When the current density is 10 $mA \cdot cm^{-2}$ and the Cu^{2+} concentration is 0.1 $mol \cdot L^{-1}$, the corrosion current density of the deposited sample reaches 1.389×10^{-5} $A \cdot cm^{-2}$, and its surface corrosion damage is reduced compared to the uncoated sample after 24 h of salt spray test. Research on the deposition mechanism indicates that Cu^{2+} undergoes instantaneous nucleation under diffusion control, tending to grow vertically and form cauliflower-like protrusions, while Ni^{2+} is discharged uniformly across the surface under electrochemical control.

Key words: Cu-Ni coatings; corrosion protection; morphology; performance

1 Introduction

In the marine environment, carbon steel structural components face severe corrosion challenges. Copper-nickel (Cu-Ni) alloys, renowned for their excellent mechanical properties[1–3], antibacterial characteristics[4–5], and corrosion resistance[6–10], are extensively employed in marine machinery, pipelines, and vessels. Researches have demonstrated that Cu-Ni alloys, with varying elemental compositions, exhibit remarkable corrosion resistance in seawater environments[11–12]. Current methods for fabricating Cu-Ni coatings on metals encompass thermal spraying[13], electrodeposition[14], laser cladding[15], etc. Among them, electrodeposition has been widely adopted for its economic efficiency and straightforward operation. Consequently, the electrodeposition of Cu-Ni film on carbon steel structures emerges as a viable solution to address the issue of seawater corrosion for workpieces.

Extensive research on the electrodeposition process of Cu-Ni alloys has a long-standing history. The properties of electrodeposited alloy coating is intricately influenced by process parameters, including electrolytic cell specifications, metal ion concentration ratios, complexing agents, electrode potential, and deposition current. Chlorides- and sulfates-based plating solutions are two prevalent systems. To circumvent the emission of chlorine gas from chloride ion oxidation in the solution as well as the equipment corrosion[16], this study used the widely employed Watt-type (sulfate) plating bath. However, employing Cu and Ni sulfate alone fails to achieve the codeposition of the two ions due to the

Received date: August 26, 2024
Foundation item: Key R&D Program of Shandong Province, China (2023SFGC0101); National Natural Science Foundation of China (51971071, 52075112, 52261135538); Fundamental Research Projects of Science & Technology Innovation and Development Plan in Yantai City (2022JCYJ023)
Corresponding author: Wang Guixiang, Ph. D., Professor, Yantai Research Institute, Harbin Engineering University, Yantai 264006, P. R. China, E-mail: wangguixiang@hrbeu.edu.cn

substantial standard reduction potential difference between Cu (+0.34 V vs. SHE) and Ni (−0.23 V vs. SHE). Consequently, the addition of a complexing agent to the plating solution is imperative to realize codeposition[17]. Various complexing agents, such as lactic acid[18], citrate, and pyrophosphate[19], have been utilized for the electrodeposition of Cu-Ni alloys. Among these, citrate, derived from biological sources, offers notable advantages: environmental friendliness, low toxicity, and high economic efficiency[20]. Citrate also serves multifunctional roles as a complexing agent, pH regulator, buffer, and brightener[21]. Therefore, unlike other complexing systems, the introduction of additional additives is unnecessary. Chassaing's[22] investigation of citric acid complexation systems under alkaline condition revealed that the discharge of Cu^{2+} was diffusion-controlled, with the proposed model accurately simulating the polarization curve results. Subsequent work by Rode et al[23] not only corroborated Chassaing's theory but also suggested novel adsorbents, highlighting that lower Cu^{2+} concentrations contribute to sustaining the stability of the plating solution. Consequently, when formulating the plating solution, it is imperative to ensure a high Ni^{2+}/Cu^{2+} ratio. Nevertheless, existing research lacks practical coating data and integrated analyses of micro-morphology and composition, which imposes certain limitations.

Many scholars have studied the ion electro crystallization theory to elucidate the formation mode of morphology. Milchev's[24–25] research on the Cu^{2+} deposition process established current-time (*I-t*) relationships under two control mechanisms: ion transfer and charge transfer. Isaev et al[26] provided precise solutions for both instantaneous and continuous nucleation processes, encompassing crystal nucleus formation and growth, whose parameters can be extracted from the initial segment of the *I-t* curve.

The purpose of this work is to develop a green and efficient surface anticorrosion technique for carbon steel. An environmentally-friendly acidic citric acid plating bath was selected to deposit Cu-Ni alloy coatings on carbon steel workpieces, and the influence of current density and Cu^{2+} concentration on the composition, morphology, and performance of the coating was examined. Additionally, this study delves into elucidating the formation mode of the deposition microstructure morphology by scrutinizing the deposition mechanism of Cu^{2+} and Ni^{2+}. The findings of this investigation provide significant reference value for developing a sophisticated Cu-Ni alloy electroplating technique and enhancing the application of Cu-Ni alloy protective coatings in marine anticorrosion.

2 Experiment

2.1 Electroplating experiment

Cu-Ni alloy coatings were electrodeposited onto cold-rolled carbon steel substrates using four distinct Cu^{2+} concentrations and four different current densities. The specific data are detailed in Table 1. pH values were adjusted to the desired levels using sulfuric acid and sodium hydroxide.

Table 1 Composition of Cu-Ni alloy plating solution and experimental conditions

Parameter	Value
$NiSO_4 \cdot 6H_2O$ concentration/g·L^{-1}	157.7
Sodium citrate concentration/g·L^{-1}	88.2
Sodium dodecyl sulfate concentration/g·L^{-1}	1
Temperature/℃	50
Time/min	10
Stirring speed/r·min^{-1}	200
Ph	5.0

Electrodeposition experiments were conducted using a constant-current power supply. The Cu^{2+} concentration ($C_{Cu^{2+}}$) and current density (*j*) parameters for each experimental group are detailed in Table 2. Each experimental group underwent deposition at least three times to ensure result reproducibility. The soluble anode comprised copper and nickel plates, while the cathode was a carbon steel sample.

Prior to experiment, the test piece was ultrasonically cleaned to remove surface grease from the carbon steel using an ethanol solution. Subsequently, 5wt% nitric acid solution was picked for acid washing to eliminate the oxide layer on the test piece surface and activate the substrate. Between each of the above steps, the test piece surface was thoroughly rinsed with deionized water to prevent the carryover of residual reagents from the preceding step to the next step.

2.2 Composition, morphology, and performance testing of coatings

The surface morphology of the coatings was observed using a scanning electron microscope (SEM), and energy dispersive spectrometer (EDS) analysis was conducted on the coating surface to delineate the elemental composition.

A digital microhardness tester was employed to assess the Vickers hardness of the prepared coating. The hardness value of the sample was calculated based on the diagonal indentation length under a 500 g load. Average value of three tests on the same sample was reported in this study.

A pin disc friction and wear tester were employed to assess the tribological performance of the coating under a load of 300 g. A friction test for 10 min was conducted and the friction coefficient of the coating surface was then calculated.

Throughout the neutral salt spray test, the temperature was kept at 35±2 ℃ and a 5wt% NaCl solution was used as the testing solution. After 24 h of testing, the test piece was retrieved from the box for SEM observation.

The contact angle tests were performed using a video optical contact angle measuring instrument. A 10 μL droplet was placed on the surface of the prepared coating and photographed. Subsequently, the contact angle of the droplets on the coating surface was calculated through computer analysis.

2.3 Electrochemical test

All electrochemical tests were carried out using a CHI760E

Table 2 Cu^{2+} concentration and current density of each experimental group

Group	A	B	C	D	E	F	G	H
$C_{Cu^{2+}}$/mol·L^{-1}	0.12	0.12	0.12	0.12	0.01	0.05	0.10	0.15
j/mA·cm^{-2}	10	15	20	30	20	20	20	20

electrochemical workstation with a conventional three-electrode system. Both electrochemical impedance spectroscopy (EIS) and polarization curve tests were performed for carbon steel and Cu-Ni alloy coatings. In this setup, the sample served as the working electrode, a saturated calomel electrode (SCE) acted as the reference electrode, and a platinum wire was employed as the counter electrode. Experiments were conducted in a 3.5wt% NaCl aqueous solution at room temperature (20 ℃). EIS and polarization curve tests were initiated when the fluctuation value of open circuit potential (OCP) was less than 5 mV over 5 min. For EIS measurements, the testing potential was set at the OCP, with a frequency ranging from 10^{-2} Hz to 10^{5} Hz and an amplitude of 5 mV. The resulting data were fitted using ZSimpWin software. The scanning speed for polarization curve testing was set at 5 mV·s^{-1}, and the voltage range was defined as ±0.3 V relative to the OCP. The corrosion current density (i_{corr}) and corrosion potential (E_{corr}) were calculated using Tafel extrapolation method.

To investigate the nucleation and growth behavior of Ni^{2+} and Cu^{2+} on a glassy carbon electrode (GCE), chronoamperometry was employed. GCE and SCE were employed as the working electrode and reference electrode, respectively, while Cu and Ni plates served as the counter electrodes for Cu^{2+} and Ni^{2+} experiments, respectively. The electrode surface area of the GCE was 0.0707 cm^2. In the chronoamperometric measurements, the potential was stepped from the OCP to the applied potential. Prior to testing, the GCE surface was polished on a polishing cloth added with nano-alumina particles to ensure experimental repeatability.

3 Results and Discussion

3.1 Microscopic morphology and composition of coating

Fig. 1 shows the morphologies of Cu-Ni alloy coatings at 5000× magnification under various current densities and Cu^{2+} concentrations. It is evident that within the current density range of 10–30 mA/cm^2, the deposits manifests as fine and densely packed cauliflower-like structures. With the escalation of current density, the morphology of these cauliflower-like protrusions becomes more pronounced. Higher deposition current density, as depicted in the figure, results in gaps between the cauliflower structures, rendering them less compact than samples with lower deposition current density. Overall, the variation in current density influences the interstices of the structure, and with increasing current density, the cauliflower-like structure transitions from a dense to a looser arrangement.

Similarly, the microstructure of the coatings was investigated under different Cu^{2+} concentrations. At very low Cu^{2+} concentrations (group E), the cauliflower-like structure transforms into sharp protrusions. However, with a further increase in Cu^{2+} concentration, the cauliflower-like structure reappears, and the structure becomes larger and looser with continuous increase in copper ions in the solution. At a specific Cu^{2+} concentration in the plating bath (group F), increasing the Cu^{2+} concentration exhibits a comparable effect to increasing the current density.

These results suggest that the formation of cauliflower-like structures requires a sufficient Cu^{2+} concentration in the plating bath. When this condition is met, augmenting the copper content will contribute to the expansion and bulging of the cauliflower-like structure. This suggests that the formation of cauliflower-like protrusions and depressions is related to the distribution of elements Cu and Ni in the coating. This connection leads to the emergence of the cauliflower-like structure in the coating when the concentration of Cu^{2+} is increased, facilitating the growth and protrusion process. This phenomenon aligns with prior studies: experiments by

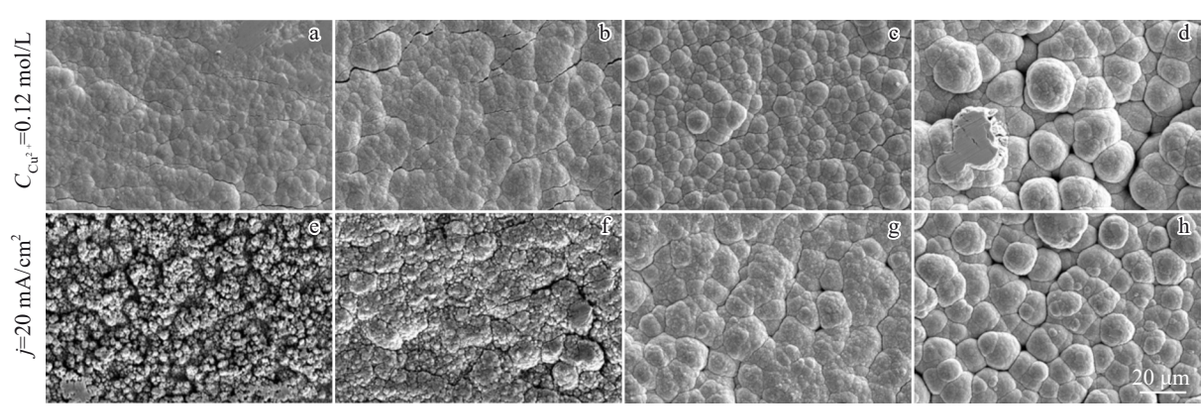

Fig.1 Morphologies of Cu-Ni coatings under different current densities (a–d) and Cu^{2+} concentrations (e–h): (a) j=10 mA/cm^2, (b) j=15 mA/cm^2, (c) j=20 mA/cm^2, and (d) j=30 mA/cm^2; (e) $C_{Cu^{2+}}$=0.01 mol/L, (f) $C_{Cu^{2+}}$=0.05 mol/L, (g) $C_{Cu^{2+}}$=0.1 mol/L, and (h) $C_{Cu^{2+}}$=0.15 mol/L

Goranova et al[27] have indicated that the Cu-Ni alloy coatings obtained through deposition form a Cu-Ni solid solution, albeit with a certain element enrichment in different structures.

To verify the element enrichment in coatings obtained by acidic citric acid system, EDS point scanning was performed on two sample groups with Cu^{2+} concentrations of 0.01 and 0.15 mol·L^{-1}. The scanning test results are shown in Fig. 2. Since the main elements in the coating are only Cu and Ni, the Ni content can be considered as 100% minus Cu content. The results indicate that in the acidic citric acid system, Cu will accumulate on the raised surfaces and Ni will accumulate in the depressions, which is not affected by the formation of cauliflower-like structure. Moreover, before the formation of cauliflower-like structures, sharp protrusions exhibit stronger Cu-enrichment ability, and the difference in Cu content between the protrusions and depressions in the group E reaches 70.92wt% . This indicates that within a wide Cu^{2+} concentration range, the formation of protrusions in the coating structure is controlled by Cu deposition.

To investigate the elemental composition of Cu-Ni alloy coatings under different current densities and Cu^{2+} concentrations, EDS mapping analyses were conducted on all samples, and the results are depicted in Table 3. As the current density changes from 10 mA·cm^{-2} to 30 mA·cm^{-2}, the Ni content in the coating gradually increases, corresponding to the progressive protrusion and dispersion of the cauliflower-like structure in the SEM images. When the Cu^{2+} concentration increases from 0.01 mol·L^{-1} to 0.05 mol·L^{-1}, a cauliflower-like structure emerges in the coating. Further increasing the Cu^{2+} concentration results in a decrease in Ni content in the coating structure, but the dispersion degree of the cauliflower-like structure do not decrease proportionally with the Ni content reduction. This indicates that changes in the cauliflower-like structure cannot be simply attributed to variations in Cu or Ni contents in the coating; instead, the current density and Cu^{2+} concentration have different effects on the cauliflower-like structure.

Based on the EDS results, it is evident that the protrusions of the cauliflower-like structure are primarily composed of Cu, indicating that the deposition behavior of Cu is the main factor controlling the cauliflower-like structure of the coating. As the concentration of Cu^{2+} in the plating bath increases, the Cu content of the coating increases, leading to the gradual formation and protrusion of cauliflower-like structures. In experimental groups A – D, the plating solution contains sufficient Cu^{2+} to ensure the formation of cauliflower-like structures. In this scenario, increasing the current density decreases Cu content in the plating layer. Since the cauliflower-like structure is primarily controlled by Cu deposition, the decrease in Cu content leads to a reduction in the number of cauliflower-like structures formed, while high current density further increases the size of cauliflower-like structures. These factors contribute to the protrusion and dispersion of cauliflower-like structures in the coating. The morphology of group D in Fig. 1 validates this hypothesis: under high current density, the coating exhibits fewer

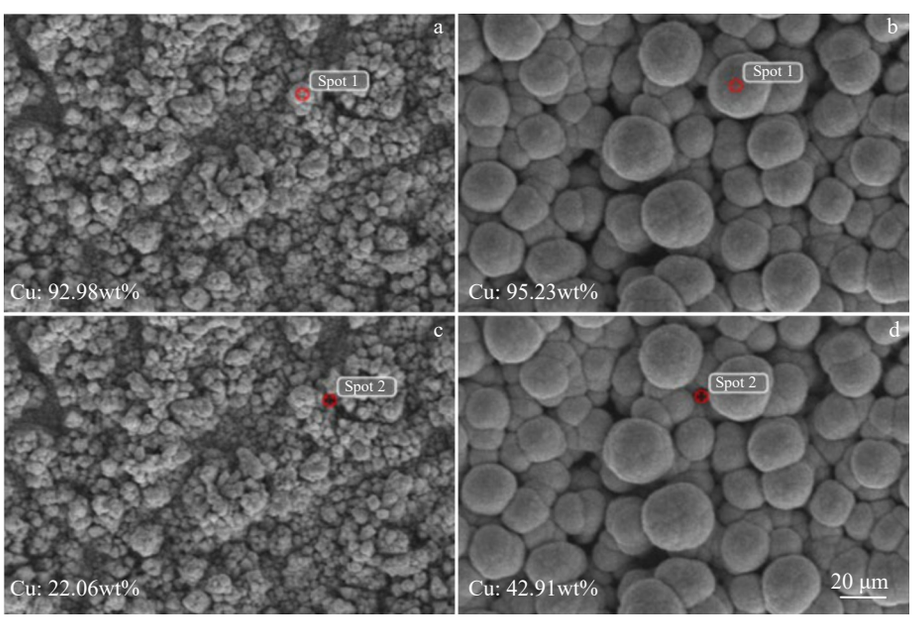

Fig.2 SEM images of two groups of samples: (a, c) group E and (b, d) group H

Table 3 Cu and Ni contents on surface of samples from different experimental groups (wt%)

Group	A	B	C	D	E	F	G	H
Cu	97.28	89.94	66.93	61.14	14.73	48.15	73.70	91.12
Ni	2.72	10.06	33.07	38.86	85.27	51.85	26.30	8.88

cauliflower-like structures with increased size.

3.2 Corrosion resistance of coating

Electrochemical tests were conducted on coatings deposited at different current densities and Cu^{2+} concentrations, and Fig. 3 illustrates the EIS and polarization curves. The electrochemical corrosion parameters of the coatings, acquired by dynamic potential polarization measurements, are presented in Table 4.

The equivalent circuit model used for impedance fitting is represented as R(Q(R(QR))), and the circuit diagram is depicted in Fig. 3e. In this model, R_s represents the solution resistance, CPE_c denotes the capacitance of the Cu-Ni coating, R_c signifies the resistance of the Cu-Ni coating, R_{ct} is the charge transfer resistance, and CPE_{dl} represents the double-layer capacitance at the interface between the Cu-Ni coating and the iron substrate.

All experimental groups exhibit Nyquist curves with one large and one small capacitive arc, aligning well with the fitting circuit represented by R(Q(R(QR))). The smaller arc radius corresponds to the film resistance R_c, representing the penetration of the corrosive media through the entire Cu-Ni alloy coating. The larger arc radius signifies the magnitude of the interface charge transfer resistance R_{ct}. Notably, the charge transfer resistance at a current density of 10 $mA·cm^{-2}$ is significantly higher than that of groups with higher current densities. This suggests that the coating deposited at a current density of 10 $mA·cm^{-2}$ is more resistant to Cl^- penetration in a Cl^- corrosive environment, thus providing enhanced protection for the iron substrate. This observation is further supported by the Bode plot, where the low-frequency modulus

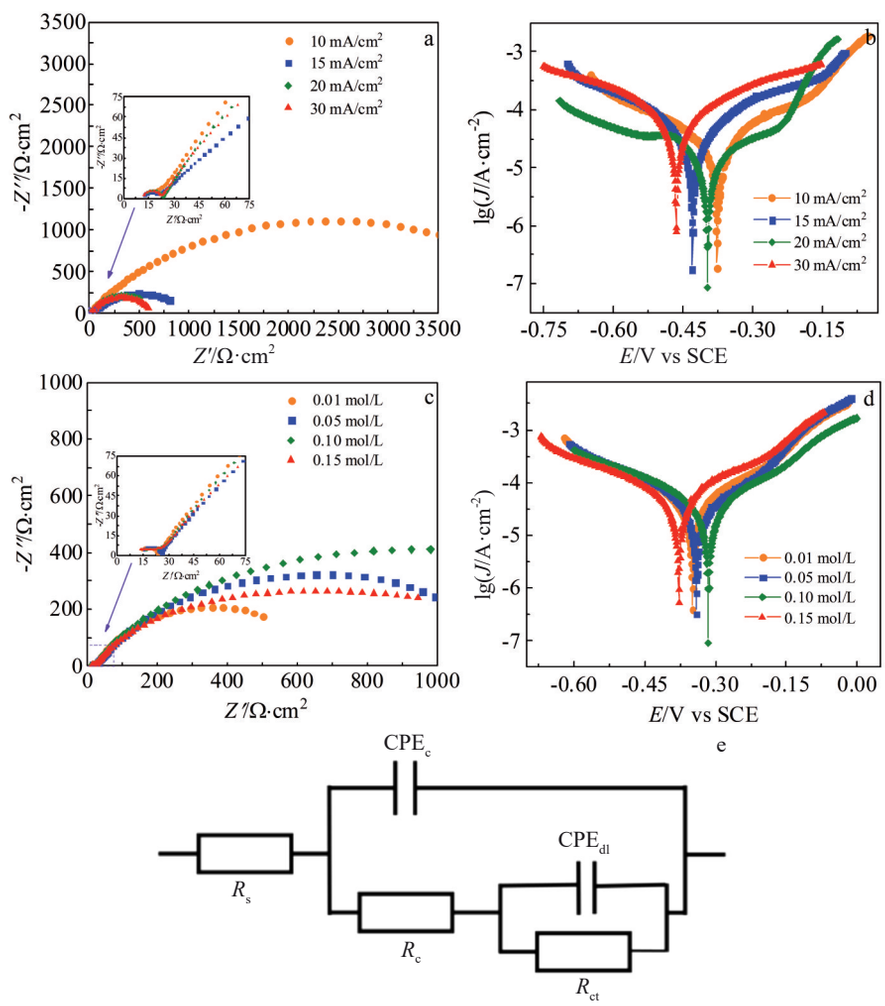

Fig.3 EIS and polarization curves of coatings under different current densities (a – b) and Cu^{2+} concentrations (c – d): (a, c) Nyquist curve, (b, d) polarization curve, and (e) circuit diagram

Table 4 Electrochemical parameters calculated from the polarization curves in Fig.3b and 3d

Group	A	B	C	D	E	F	G	H
E_{corr}/V	−0.377	−0.430	−0.397	−0.464	−0.315	−0.349	−0.341	−0.378
$i_{corr}/\times10^{-5}$ A·cm^{-2}	3.536	3.599	4.234	7.416	8.379	5.808	4.711	6.908

values of the experimental group with a current density of 10 mA·cm^{-2} show significant improvement compared to other groups, indicating overall higher corrosion resistance of the coating. Electrochemical parameters calculated from the polarization curves further indicate that reducing the current density leads to a decrease in corrosion current density (i_{corr}) of the coating: the corrosion current density of the coating changes from 3.536×10^{-5} A·cm^{-2} to 7.416×10^{-5} A·cm^{-2}. This implies that, when exposed to corrosive media, samples with low current densities are less susceptible to corrosion damage and exhibit higher corrosion resistance, which can be attributed to the higher Cu content. Additionally, the microstructure of the coating plays a crucial role: higher current density results in larger cauliflower-like structures with increased gaps between them. In comparison to dense and compact structures under low current density, larger gaps facilitate the entry and exit of corrosive ions, making ion penetration easier and accelerating material corrosion. This is consistent with the electrochemical test results, where samples with high current density exhibit lower charge transfer resistance and impedance modulus values.

The EIS and polarization curves of coatings deposited at different Cu^{2+} concentrations reveal that the corrosion resistance of the coatings does not change monotonically with Cu^{2+} concentration in the plating bath. Calculation of corrosion current density from polarization curves indicates that with increasing the Cu^{2+} concentration from 0.01 mol/L to 0.15 mol/L, the corrosion current density of the coating changes from 8.379×10^{-5} A·cm^{-2} to 6.908×10^{-5} A·cm^{-2}. The coating exhibits the highest corrosion resistance at a Cu^{2+} concentration of 0.1 mol·L^{-1}. This phenomenon can be explained by analyzing the microstructure. When the Cu^{2+} concentration is below 0.05 mol·L^{-1}, the coating comprises sharp protrusion structures. Due to the low Cu content in the plating solution, the deposition of Cu-rich protrusions is relatively restricted, resulting in a sparse coating structure that offers inadequate protection against corrosive media and low corrosion resistance. As the Cu^{2+} concentration exceeds 0.05 mol/L, a cauliflower-like structure begins to emerge in the coating. With further increasing Cu^{2+} concentration, the cauliflower-like structure gradually replaces all sharp protrusions, forming a dense cauliflower-like structure with the highest corrosion resistance. As the Cu^{2+} concentration continues to increase, gaps form between cauliflower-like structures, leading to a transition from dense coating structures to sparse ones. This transition adversely affects corrosion resistance, outweighing the increase in Cu content in the coating, and resulting in a reduction in capacitance arc radius and an increase in corrosion current density in the polarization curve. Additionally, it is observed that when the Cu^{2+} concentration exceeds 0.1 mol·L^{-1}, variations in sample impedance and polarization curve test results due to changes in Cu^{2+} concentration become relatively small. This suggests that the impact of the transformation from sharp protrusions to cauliflower-like structure on corrosion resistance is more significant than the effect of the cauliflower-like structure itself.

The electrodeposition parameters of the group with the optimal corrosion resistance in the previous tests were chosen: a current density of 10 mA·cm^{-2} and a Cu^{2+} concentration of 0.1 mol/L. Comparative results with the uncoated carbon steel matrix are depicted in Fig. 4, illustrating the macroscopic and 2000× microscopic morphologies of sample after salt spray exposure for 24 h. Fig. 4e displays the polarization curve, while Table 5 presents the electrochemical corrosion parameters of the Cu-Ni coating calculated through potentiodynamic polarization measurements. The corrosion potential of the prepared Cu-Ni coating shifts forward by approximately 0.2 V, and the corrosion current density decreases by an order of magnitude. Salt spray experiments confirm that under the same NaCl concentration, Cu-Ni coatings exhibit superior resistance to corrosion damage. This substantiates that electrodepositing Cu-Ni coatings on carbon steel structural components effectively mitigates corrosion losses in seawater environments, thereby expanding the

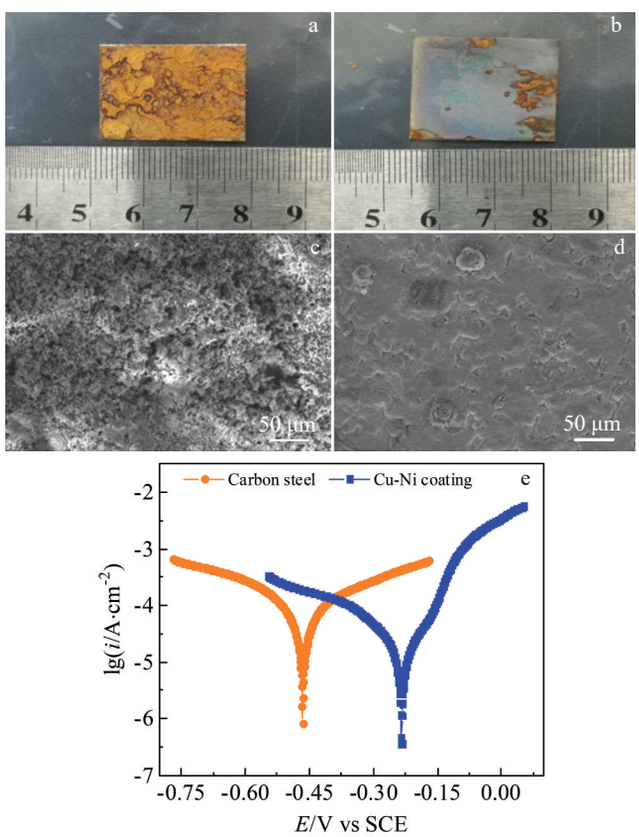

Fig.4 Comparison of macro appearances (a – b), microscopic morphologies (c–d), and polarization curves (e): (a, c) carbon steel and (b, d) Cu-Ni coating

Table 5 Electrochemical parameters calculated from the curves in Fig.4e

Sample	E_{corr}/V	I_{corr}/A·cm^{-2}
Carbon steel	−0.466	1.001×10^{-4}
Cu-Ni coating	−0.234	1.389×10^{-5}

application of carbon steel structural components in the marine field to a certain extent.

3.3 Mechanical properties and surface properties of coatings

Vickers hardness tests were performed on samples deposited at various current densities and Cu^{2+} concentrations, and the results are illustrated in Fig. 5a and 5c. Fig. 5b and 5d depict the tribological test outcomes for samples deposited at different current densities and Cu^{2+} concentrations. Upon comparing Fig. 5a and 5c, it is evident that the hardness of the coating is not significantly influenced by the current density. This may be due to the minimal effect of current density on the Ni content in the coating. Another explanation is that the density of the cauliflower-like structure is not the primary factor affecting the Vickers hardness of the coating. As observed in Fig. 5c, with increasing the Cu/Ni ratio in the plating bath, the overall hardness of the coating exhibits a decreasing trend, which is attributed to the inherent properties of copper and nickel. The electrodeposited Cu-Ni alloy forms a solid solution, and the two metals can form an infinite solid solution. Copper, as a wear-resistant material, possesses good ductility but lower hardness than nickel. As the Cu content in the coating gradually increases, the hardness inevitably decreases. However, slight variations in Vickers hardness are observed between Cu^{2+} concentrations of 0.1 and 0.15 $mol \cdot L^{-1}$, even though SEM observations has confirmed the formation of a cauliflower-like structure at this point. This indicates that the sharp protrusion structure at low Cu^{2+} concentrations contributes more to hardness than the cauliflower-like structure. Once the coating structure transitions completely from sharp protrusion to cauliflower-like structure, the overall hardness no longer changes significantly.

The curve in Fig. 5b indicates that increasing the deposition current density generally leads to an increase in friction coefficient of the coating. Combined with microstructure analysis, it becomes evident that the augmented gaps in cauliflower-like structures contribute to higher surface roughness of the coating. However, EDS mapping tests on the coating reveal that in this scenario, the Cu content of the coating gradually decreases. This implies that the impact of structural changes on the wear resistance of the coating outweighs the contribution of the wear-resistant metal Cu in the binary alloy coating.

In Fig. 5d, the experimental group with a Cu^{2+} concentration of 0.01 $mol \cdot L^{-1}$ exhibits a high friction coefficient at the beginning of the friction test, and the friction coefficient undergoes a sharp change as the experiment progresses. Microstructure analysis indicates that the sharp protrusion structure is rougher than the cauliflower-like structure, and the lower Cu content in the coating results in the absence of a wear-resistant Cu-rich phase. These factors collectively contribute to the overall friction coefficient of the coating being significantly higher than that of other experimental groups. However, after a period of wear, the difference in friction coefficient among the remaining experimental groups is not significant, suggesting that, similar to hardness, changes in cauliflower-like structure have little effect on wear resistance.

To further investigate the impact of the process parameters on surface properties, water contact angle tests were conducted on samples deposited at different current densities and Cu^{2+} concentrations, and the results are depicted in Fig. 6. It is observed that the water contact angle of the coating does

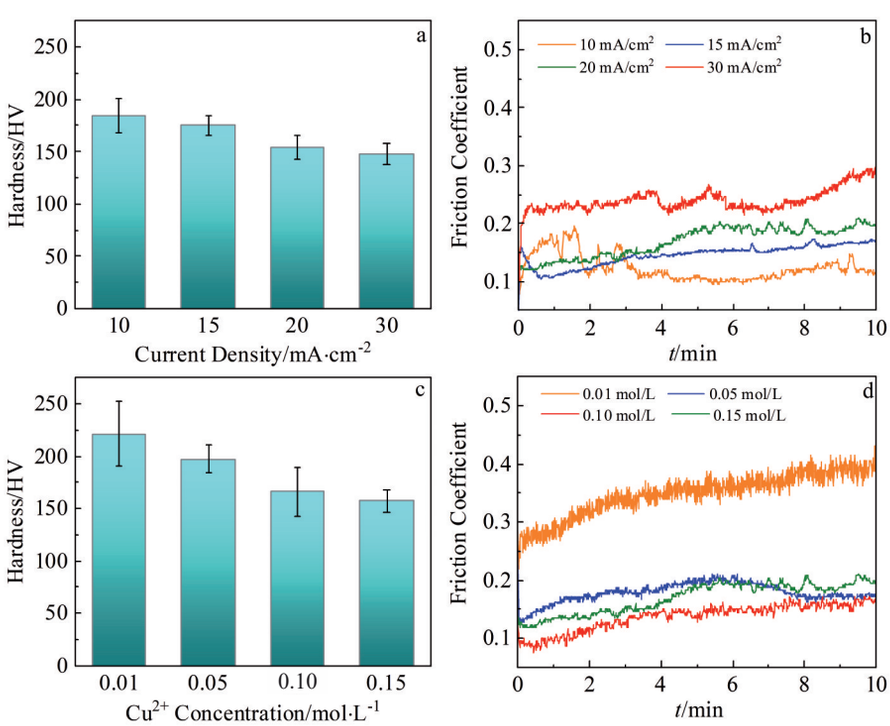

Fig.5 Vickers hardness (a, c) and friction coefficient curves (b, d) of coatings at different current densities and Cu^{2+} concentrations

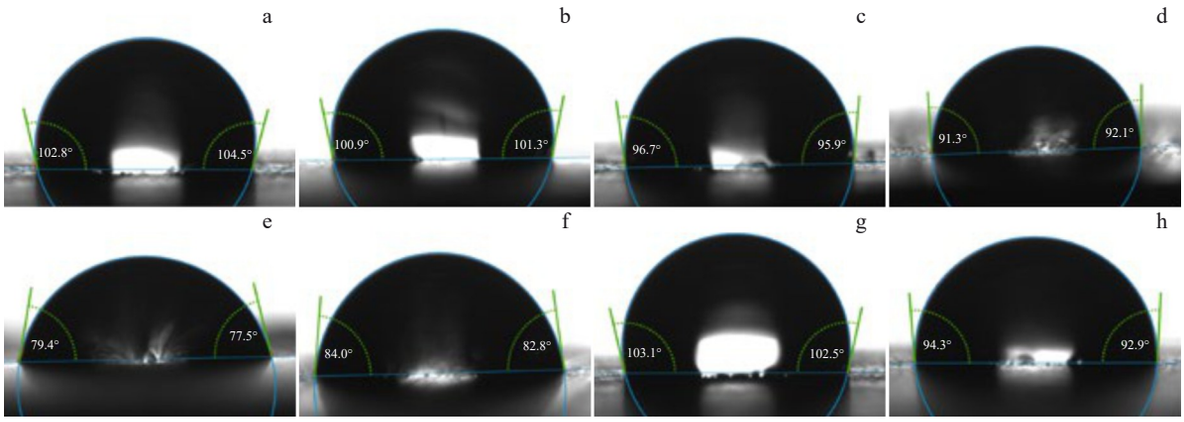

Fig.6 Water contact angle of coatings at different current densities and Cu^{2+} concentrations: (a) group A, (b) group B, (c) group C, (d) group D, (e) group E, (f) group F, (g) group G, and (h) group H

not change significantly under different current densities but generally decreases with increasing current density. The coating structure deposited at high current densities has larger microscopic dimensions, and the sparse structure leads to a rough surface, resulting in a slight decrease in its hydrophobicity.

When the Cu^{2+} concentration is varied, the water contact angle changes more significantly, with a notable decrease observed at extremely low Cu^{2+} concentrations. This suggests that the sharp protrusion structure of the coating contributes far less to surface hydrophobicity than the cauliflower-like structure, and the substantial difference between the two structures results in a significant variance in hydrophobicity. Furthermore, the water contact angle test results align well with the previous electrochemical tests. The hydrophobicity of the coating affects its ability to block the infiltration of corrosive media to some extent, thereby impacting its corrosion resistance.

3.4 Electro crystallization mechanism

A plating bath with a Cu^{2+} concentration of 0.1 mol·L^{-1} was selected as the electrolyte to investigate the electro crystallization mechanism of Cu^{2+} and Ni^{2+}. The deposition type of Cu^{2+} and Ni^{2+} can be determined by analyzing the current-time (*J*-*t*) relationship during the initial nucleation process[28]. When J^n-*t* follows a linear relationship, the nucleation type is classified into categories based on the value of *n*. When crystal growth is controlled by electron transfer, the system is instantaneous nucleation if n=1/2, and continuous nucleation if n=1/3. When crystal growth is controlled by the reactant ion transfer, the system is instantaneous nucleation if n=2, and continuous nucleation if n=2/3.

The applied potential in both systems is slightly negative relative to the deposition potential, and the potential gradually increases from the OCP to the target potential. Fig. 7a illustrates the transient current density curves of Cu^{2+} under different applied potentials, while Fig. 7b presents the logarithmic relationship curve of the early-stage transient current and time. The steady-state current exhisits no significant overall change, suggesting stable current values across different applied potentials. This indicates that the deposition of Cu^{2+} is controlled by diffusion steps. The curve at an applied potential of −0.9 V effectively demonstrates the initial nucleation behavior of Cu^{2+} deposition, revealing that copper deposition in this system follows diffusion-controlled instantaneous nucleation. Fig. 7c depicts the transient current curves of Ni^{2+} under different applied potentials, and Fig. 7d shows the logarithmic relationship curve of the early-stage transient current and time. The notable difference in steady-state current under various deposition potentials indicates that the deposition of Ni^{2+} is controlled by electrochemical steps. According to the curve at a deposition potential of −1.4 V, it can be determined that the deposition mode of Ni^{2+} is electrochemically-controlled instantaneous nucleation.

The coating microstructure can now be elucidated based on the initial nucleation behavior of ions. The distinct deposition mechanisms of Cu and Ni not only give rise to the unique morphology of Cu-Ni alloy coatings, but also lead to variations in current density that impacts the composition of the coatings.

The deposition of Cu is diffusion-governed, making copper growth more sensitive to variations in plating bath concentration. In regions with favorable diffusion, copper deposition is preferentially initiated, manifesting as vertically grown crystals at higher copper content in the coating, which ultimately evolves into a cauliflower-like structure. The Cu content in the alloy coating is substantially influenced by the deposition behavior of other metal component. The deposition of Ni is electrochemically-governed and remains unaffected by diffusion limitations. Ni nucleates at charge transfer sites, exhibiting a planar growth propensity. It is evident that there is a higher nickel concentration in the bottom layer and depressions within the coating. Additionally, owing to the considerably higher nickel content in the plating bath relative to copper, nickel ions in the solution that are not complexed with citric acid lack preferential nucleation sites, resulting in random nucleation. Furthermore, this mechanism is further validated by the observation that current density directly influences the deposition of Ni: increasing current density leads to a significant rise in Ni content in coating.

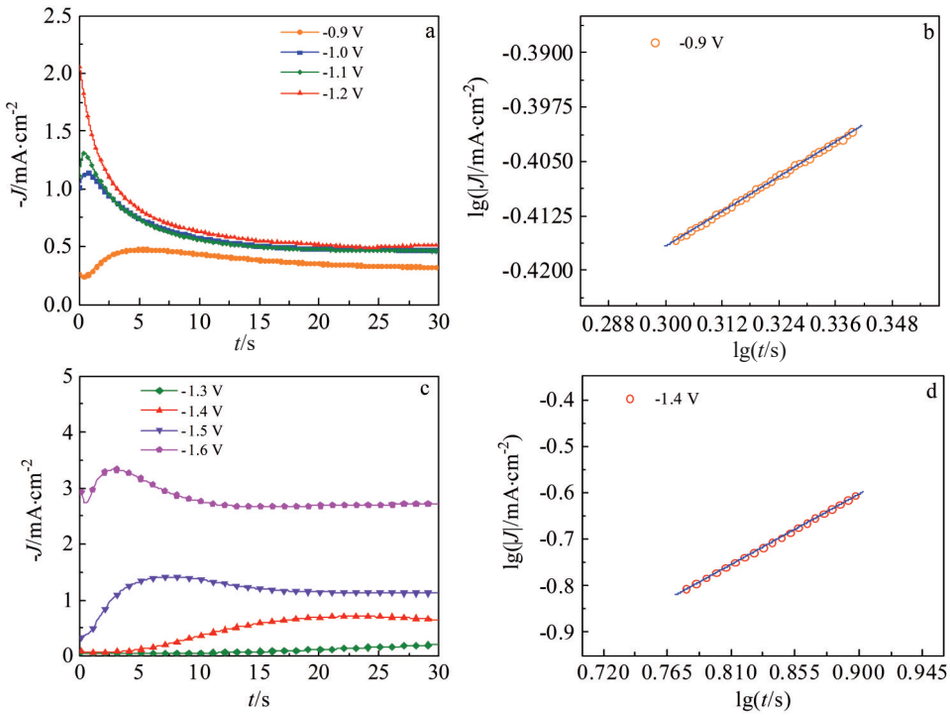

Fig.7 Current-time (*J*-*t*) curves (a, c) and early-stage lg*J*-lg*t* curves (b, d) of Cu^{2+} and Ni^{2+}: (a–b) Cu^{2+} and (c–d) Ni^{2+}

4 Conclusions

1) The Cu-Ni alloy coatings exhibit a prevailing cauliflower-like structure, whose morphological characteristics are influenced by current densities and Cu^{2+} concentrations. This coating effectively prevents the corrosion damage of Cl^- to the substrate, with the minimum corrosion current density of 1.389×10^{-5} A·cm^{-2}. After 24 h of salt spray testing, the corrosion area of the coated sample is significantly smaller than that of the sample without coating coverage.

2) Changing the current density and Cu^{2+} concentration enables the preparation of Cu-Ni alloy coatings with different properties. With increasing the deposition current density, the corrosion current density of the coating changes from 3.536×10^{-5} A·cm^{-2} to 7.416×10^{-5} A·cm^{-2}, and both hardness and hydrophobicity show a decreasing trend. With increasing Cu^{2+} concentration from 0.01 mol/L to 0.15 mol/L, the corrosion current density of the coating changes from 8.379×10^{-5} A·cm^{-2} to 6.908×10^{-5} A·cm^{-2}, while hardness and wear resistance generally decrease.

3) The protrusions in the coating microstructure are Cu-rich, while the depressions are Ni-rich. The Cu^{2+} deposition follows diffusion-controlled instantaneous nucleation, while the Ni^{2+} deposition adheres to electrochemically-controlled instantaneous nucleation.

References

1 Pellicer E, Varea A, Pané S *et al. Surf Coat Technol*[J], 2011, 23–24(205): 5285

2 Zhang X Y, Ma Y, Lin N M *et al. Surf Coat Technol*[J], 2013, 232: 515

3 Alizadeh M, Safaei H. *Appl Surf Sci*[J], 2018, 456: 195

4 Wang Y, Lu X X, Yuan N Y *et al. Alloys Compd*[J], 2020, 849: 156222

5 Silva F D, Cinca N, Dosta S *et al. Surf Coat Technol*[J], 2019, 361: 292

6 Song R X, Zhang S H, He Y *et al. Colloids and Surfaces A: Physicochemical and Engineering Aspects*[J], 2022, 649: 129427

7 Lin Z F, Zhang W, Zhang W *et al. Mater Chem Phys*[J], 2022, 277: 125503

8 Zhang P Y, Meng G Z, Wang Y Q *et al. Corrosion Communications*[J], 2021, 2: 72

9 Deo Y, Guha S, Sarkar K *et al. Appl Surf Sci*[J], 2020, 515: 146078

10 Rajasekaran N, Mohan S. *J Appl Electrochem*[J], 2009, 39(10): 1911

11 Yuan S G, Pehkonen S O. *Corros Sci*[J], 2007, 49(3): 1276

12 Ismail K M, Fathi A M, Badawy W A. *Corros Sci*[J], 2006, 48(8): 1912

13 Jang J M, Lee H S, Singh J K. *Materials*[J], 2021, 13(24): 5776

14 Goranova D, Avdeev G, Rashkov R. *Surf Coat Technol*[J], 2014, 240: 204

15 Yang Y, Wang A H, Xiong D H *et al. Surf Coat Technol*[J], 2020, 384: 125316

16 Pingale A D, Owhal A, Katarkar A S *et al. Materials Today: Proceedings*[J], 2021, 47: 3301

17 Silaimani S M, Vivekanandan G, Veeramani P. *International Journal of Environmental Science and Technology*[J], 2015, 12(7): 2299

18 Kamel M M, Anwer Z M, Abdel-Salam I T *et al. Surf Interface*

Anal[J], 2014, 46(7): 442
19 Chia P Y, Haseeb A, Mannan S H. *Materials*[J], 2016, 9(6): 430
20 Ghosh S K, Grover A K, Dey G K *et al. Surf Coat Technol*[J], 2000, 126(1): 48
21 Green T, Russell A, Roy S. *J Electrochem Soc*[J], 1998, 145(3): 875
22 Chassaing E, Quang K V, Wiart R. *J Appl Electrochem*[J], 1987, 17: 1267
23 Rode S, Henninot C, Vallières C *et al. J Electrochem Soc*[J], 2004, 151(6): C405
24 Milchev A, Zapryanova T. *Electrochim Acta*[J], 2006, 51(14): 2926
25 Milchev A, Zapryanova T. *Electrochim Acta*[J], 2006, 51(12): 4916
26 Isaev V A, Grishenkova O V, Zaykov Y P. *J Electroanal Chem*[J], 2018, 818: 265
27 Goranova D, Rashkov R, Avdeev G *et al. Journal of Materials Science*[J], 2016, 51(18): 8663
28 Kong D L, Zheng Z, Meng F Y *et al. J Electrochem Soc*[J], 2018, 165(16): D783

电流密度和铜离子浓度对电沉积Cu-Ni镀层性能的影响

郭叙言[1]，熊壮壮[1]，王桂香[1,3]，周　强[1]，武艳雄[1]，孔德龙[2]，马福秋[1]，巫瑞智[3]
(1. 哈尔滨工程大学 烟台研究院，山东 烟台 264006)
(2. 枣庄学院 化学化工与材料科学学院，山东 枣庄 277160)
(3. 哈尔滨工程大学 超轻材料与表面技术教育部重点实验室，黑龙江 哈尔滨 150001)

摘　要：研究了一种简单、高效、环保的防腐技术，通过在工件表面沉积Cu-Ni合金涂层来阻止腐蚀介质，从而保护碳钢表面免受腐蚀。使用扫描电子显微镜、X射线能量色散光谱、维氏硬度计、摩擦磨损试验机和电化学测试研究了电流密度和Cu^{2+}浓度对涂层成分、形态和组成的影响。结果表明，涂层表面出现花椰菜状富镍突起结构。较低的电流密度和Cu^{2+}浓度通过影响晶粒微观结构和Cu/Ni含量来影响涂层的维氏硬度和耐磨性，从而导致硬度和耐磨性能的降低。当电流密度为10 mA·cm^{-2}，Cu^{2+}浓度为0.1 mol·L^{-1}时，沉积样品的腐蚀电流密度达到1.389×10^{-5} A·cm^{-2}。经过24 h的盐雾试验后，镀层表面腐蚀损伤明显小于未覆盖镀层样品。对沉积机理的研究表明，Cu^{2+}在扩散控制下经历瞬时形核，倾向于垂直生长并形成花椰菜状突起，而Ni^{2+}则受电化学控制，在表面均匀放电。

关键词：Cu-Ni镀层；腐蚀防护；形态；性能

作者简介：郭叙言，男，1999年生，硕士，哈尔滨工程大学烟台研究院，山东 烟台 264006，E-mail：gxy321517181@hrbeu.edu.cn